A Simple Predictive Model for Spherical Indentation

Article · February 1993

DOI: 10.1557/JMR.1993.0297

2 authors, including:

Michael V Swain
University of Otago
686 PUBLICATIONS **22,924** CITATIONS

SEE PROFILE

A simple predictive model for spherical indentation

J. S. Field
Department of Mechanical Engineering, University of Sydney, New South Wales, 2056, Australia

M. V. Swain
CSIRO Division of Applied Physics, Lindfield, New South Wales, 2070, Australia

(Received 13 July 1992; accepted 28 September 1992)

A simple model is described with which the entire force versus penetration behavior of indentation with a sphere, during loading and unloading, may be simulated from knowledge of the four test material parameters, Young's modulus, Poisson's ratio, flow stress at the onset of full plastic flow and strain hardening index, and the elastic properties of the indenter. The underlying mechanisms are discussed and the predictions of the model are compared with data produced by an ultra low load, penetration measuring instrument.

I. INTRODUCTION

Load cycle indentation, which produces plots similar to that typical for steel shown in Fig. 1(a), is being used increasingly to investigate the mechanical properties of material where the depth of penetration must be small. The plots basically reflect the interaction of the indenting process with the four test material properties, Young's modulus, Poisson's ratio, initial flow stress and strain hardening, and the elastic properties of the indenter.

Indentation may be wholly elastic, elastic/plastic, or wholly plastic, and the mix of these responses is subtly reflected in the shape of the plots. Consequently, understanding their significance and estimating materials properties from them require a suitable model of the indentation process.

The expressions developed in this paper model load cycle indentation with a spherical indenter and are applicable to any mix of elastic /plastic behavior. The model is limited only by the requirement that the radius of the circle of indenter contact must be less than the spherical radius of the indenter. Loads are increased and decreased in discrete steps and force equilibrium is assumed at each step.

Load cycle plots are generated by an implementation of the model on an ordinary IBM compatible PC. Modeled load cycles plots may be compared with ones produced by a UMIS-2000 ultra-micro-indentation system developed by the Division of Applied Physics of CSIRO in Australia.[1]

The UMIS-2000 also allows indentation with multiple partial unloading, producing plots similar to Fig. 1(b), also typical of steel. This technique permits the elastic and plastic components of indentation to be separated and hardness and elastic modulus to be calculated at each step as a function of penetration. This technique is also included and modeled. Multiple partially unloaded data plots may also be compared with ones produced by the UMIS-2000 and with examples of a hardness and modulus plot derived from them.

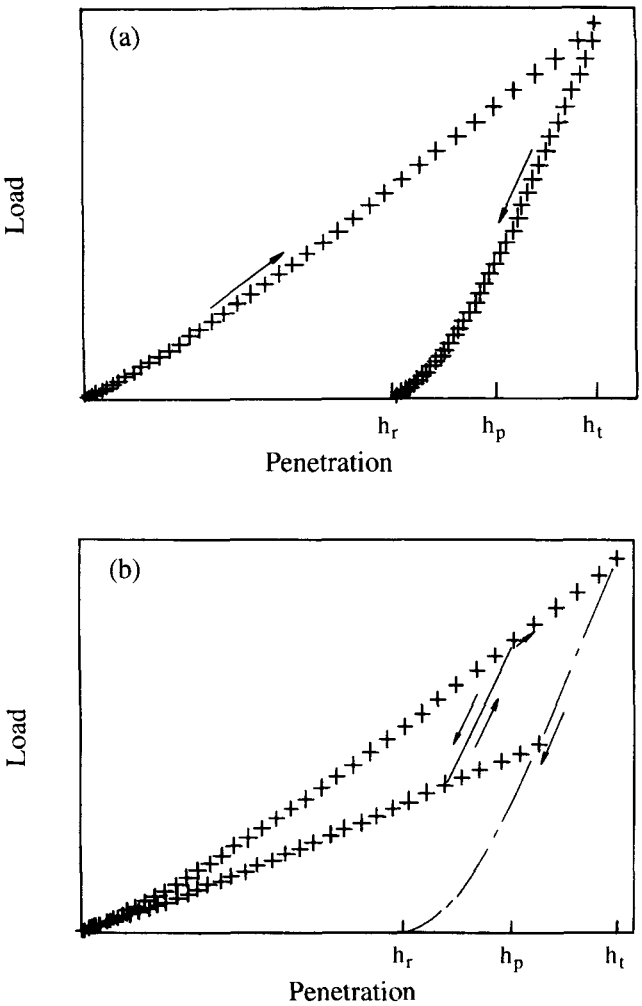

FIG. 1. (a) Load cycle plot typical of an elastic/plastic material such as steel. (b) Multiple partial unloading plot typical of an elastic/plastic material such as steel.

Peripheral issues that will also be discussed include selection of optimum indenting conditions, estimation of material parameters, the effects of departure of the indenter from perfect geometry, the stress strain behavior of materials near the onset of first yielding, and the disposition of material displaced by indentation.

II. THE MECHANISMS OF INDENTATION

Early attempts to model elastic/plastic indentation concentrated on wedge indenters and the analysis of slip line fields—see, for example, Hill, Lee, and Tupper.[2] However, these methods have not proved to be particularly successful and have now been generally abandoned—see Samuels.[3] Recognizing the difficulties with slip line techniques, phenomenological models were proposed by Shaw and DeSalvo[4] and Mulhearn.[5]

Developing these models, Francis[6] argued that in an ideal plastic solid undergoing spherical indentation, full plastic flow develops in three stages characterized by the value of P_m/Y, where P_m is the mean pressure over the circle of contact and Y is the yield stress in simple tension or compression. While P_m/Y is less than 1.1, the stress is insufficient to initiate plastic flow, deformation is wholly elastic, and complete recovery occurs on unloading.

When P_m/Y reaches 1.1 yielding is initiated in a localized region, below the center of the contact area. With further loading, this region enlarges but remains totally enclosed by elastically strained material until P_m/Y approaches 3.0 when it begins to involve the free surface.

Throughout the range $P_m/Y = 1.1$ to $P_m/Y = 3.0$, plastic flow at the surface is constrained and the radius of the circle of indenter contact is determined by elastic deformation. Some subsurface plastic deformation is possible, however; at first as a result of deformation in the elastic hinterland and then, as P_m/Y approaches 3.0, by uplifting of the free surface, but the effect of this on such measurable quantities as mean pressure is very small.

Recovery is incomplete when the indentation is unloaded during this stage as residual elastic stresses are unable to reverse the plastic strains.

When P_m/Y reaches 3.0, full plastic flow allows the radius of the circle of contact to grow at a rate sufficient to maintain a constant value of P_m/Y. Unloading during this stage leaves a permanent residual depression related in size to the maximum load applied.

Materials that strain harden appear to follow a similar pattern, although strain hardening delays the onset of plastic flow and modifies the relationship between load and the circle of contact radius once plastic flow has fully developed.

These mechanisms are consistent with much of the experimental evidence and are used as a basis for the present work. More complete modeling using finite element methods may in the future provide further insights—see, for example, Follansbee and Sinclair,[7] but these are not as yet as convenient to use.

III. THE BASIS OF A SPHERICAL INDENTATION MODEL

Stepwise indentation is an equilibrium process; at each step load is supported by reaction forces arising from elastic deformation of material surrounding the indentation. Some frictional forces at the indenter interface may also contribute, but these have been ignored.

The total depth of penetration of a sphere into an elastic half space is given by Johnson[8] as

$$\delta = Qk \tag{1}$$

where

$$Q = (9/16)^{1/3}(P/E^*)^{2/3} \tag{2}$$

and

$$k = (1/R)^{1/3} \tag{3}$$

In these P is the load, $1/R$ is the curvature of the contact surfaces (i.e., R is the radius of the indenter), and

$$1/E^* = (1 - \nu_m^2)/E_m + (1 - \nu_i^2)/E_i \tag{4}$$

in which ν_m and E_m are Poisson's ratio and Young's modulus for the material of the semi-infinite body and ν_i and E_i are Poisson's ratio and Young's modulus for the indenter material, respectively.

Sneddon[9] showed that elastic displacements of a plane surface above and below the circle of contact are equal for wholly elastic loading, as illustrated schematically in Fig. 2(a). This idea is central to the model and will be used several times during its development.

Where penetration is small compared with the spherical radius of the indenter, the relationship between depth of penetration and the radius of the circle of contact is approximately

$$\delta = a^2/R \tag{5}$$

The mean pressure over the circle of contact is

$$P_m = P/\pi a^2. \tag{6}$$

Using Eqs. (1) to (6), a critical load corresponding with the onset of full plastic flow in materials that do not work harden may be obtained in the form

$$P = (9/16)(R/E^*)^2(3\pi Y)^3 \tag{7}$$

Tabor[10] showed that results obtained for perfectly plastic solids may be applied to materials that strain harden providing Y is replaced by a representative flow stress Y_r related to some representative strain ϵ_r.

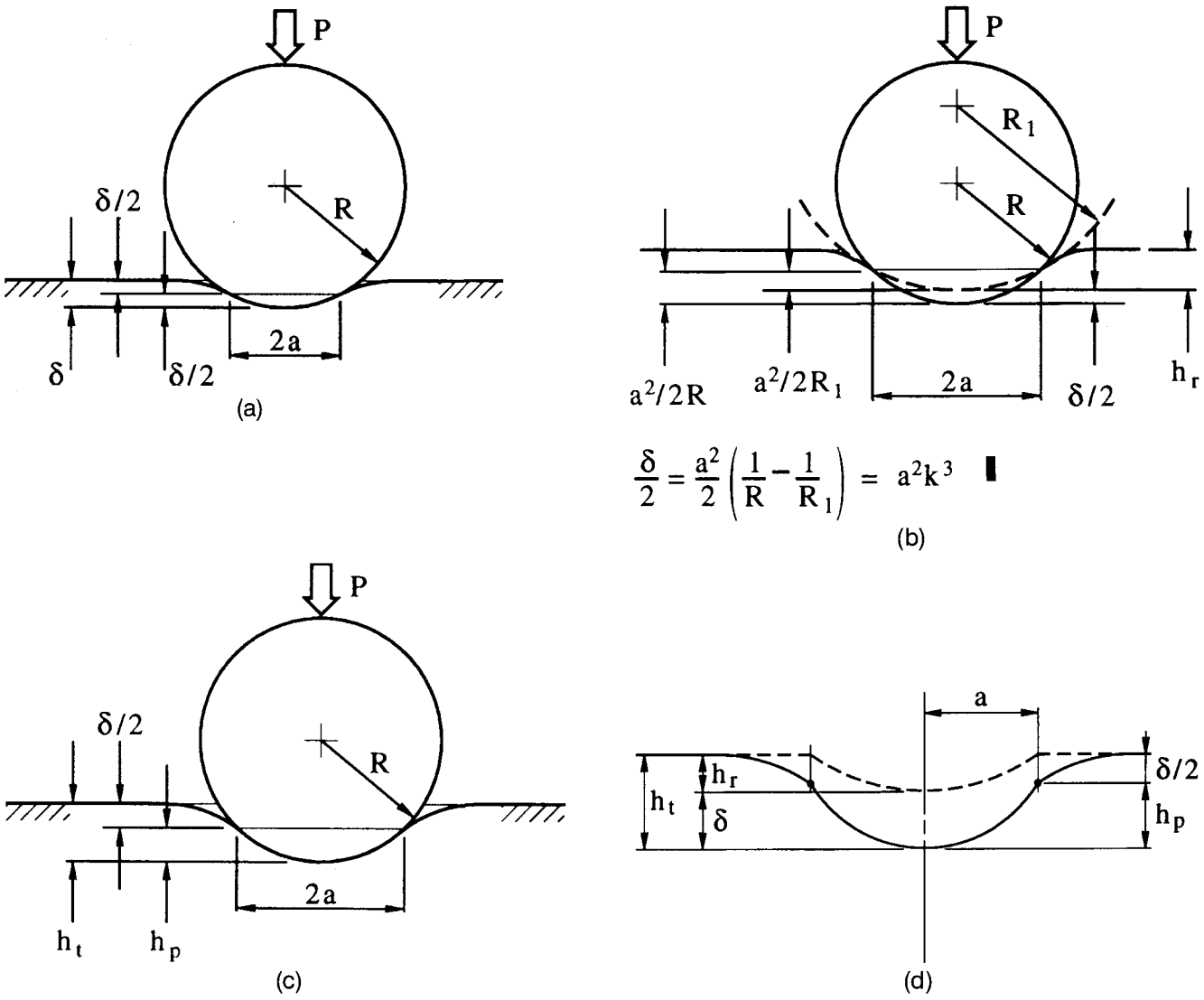

FIG. 2. (a) Schematic geometry of elastic indentation of a plane surface with a smaller spherical indenter. (b) Schematic geometry of elastic loading of a preformed spherical impression. (c) Schematic geometry of elastic/plastic indentation. (d) Schematic relationship between the depth of loaded and unloaded indentations.

Drawing on a number of sources, Francis[6] showed that in the range $P_m/Y_r = 1.1$ to $P_m/Y_r = 3.0$, P_m/Y_r correlates linearly with $\mathrm{Ln}(E^*a/Y_rR)$. This result is difficult to incorporate into a model as there is no way of determining the extent of plastic strain ϵ_r or the value of Y_r as plastic flow develops. However, we may proceed by assuming that the radius of the circle of contact is determined by elastic deformation alone up to $P_m/Y_r = 3.0$ at which point a transition to full plastic flow occurs.

Tabor[10] showed that

$$\epsilon_r = 0.2 \tan \beta \tag{8}$$

is an appropriate expression for representative strain in conical (and pyramidal) indentation where β is the angle between the indenter flank and the original surface.

In spherical indentation, strain increases continuously with indentation size, and an appropriate equivalent expression is

$$\epsilon_r = 0.2\ a/R \tag{9}$$

where $\tan \beta \approx \sin \beta \approx a/R$.

Although Tabor[10] showed this expression to be valid down to $a/R = 0.23$ (for a steel specimen), it may be necessary to place a limit on its validity below this. However, it seems unlikely that its validity will be seriously in question while P_m/Y_r remains equal to 3.0.

For ductile materials stress strain curves are often well described by the power law relationship

$$Y = Y_0(\epsilon/\epsilon_0)^x \tag{10}$$

proposed by Nadai[14] where Y_0 and ϵ_0 are material constants. This allows the flow stress at some higher strain to be calculated from the values pertaining at the onset of yielding, providing the strain hardening index x is known.

At the onset of full plastic flow, mean pressure is related to the circle of contact radius and to representative flow stress by $P_m = P_c/\pi a_c^2 = 3Y_c$ in which the subscripts now indicate critical values. Additionally, the total penetration at this point is related to the circle of contact radius by $\delta_c = a_c^2/R$. The representative flow stress Y_c is associated with a representative strain ϵ_c which has accumulated to this point by $Y_c = Y_0(\epsilon_c/\epsilon_0)^x$.

At the onset of full plastic flow the representative strain is therefore

$$\epsilon_c = 0.2\ a_c/R \tag{11}$$

and the plastic flow onset load is

$$P_c = 3\pi a_c^2 Y_c \tag{12}$$

Introducing Nadai's equation, this becomes

$$P_c = 3\pi a_c^{2+x} Y_0 (0.2/\epsilon_0 R)^x \tag{13}$$

A similar equation may be obtained for a load P', greater than P_c, at which the radius of the circle of contact is a' but with all other terms unchanged. Forming a ratio between these loads, the radius of the circle of contact at P' is

$$a' = a_c(P'/P_c)^{1/(2+x)} \tag{14}$$

This is similar to Meyer's[15] relationship between the radius of the circle of contact and load which is normally given in the form

$$a = kP^{1/m} \tag{15}$$

where $m = x + 2$, as proposed by Tabor.[10]

This relationship allows the model to be extended into the region of full plastic flow.

The residual impression remaining when an indentation is unloaded from beyond the onset of full plastic flow is approximately spherical with a spherical radius large compared to that of the indenter. The chordal diameter of the impression at the surface is similar to that of the loaded indentation, but its depth is reduced by elastic recovery. Indentation beyond the onset of full plastic flow is therefore equivalent to reloading a preformed impression into reconformation with the indenter, the total penetration being the sum of the depth of the residual impression and the elastic displacement associated with its reloading.

Unloading may be treated in a similar manner, the partially recovered penetration at a reduced load being the sum of the depth of a residual impression and the elastic displacement arising from its *partial* reloading.

The problem of loading a preformed spherical impression was analyzed by Goodman and Keer.[11] The equations used in this paper are, however, based on the earlier work of Love[12] and are as described by Puttock and Thwaite.[13] The solution in this form is similar to that for the elastic loading of a plane but using relative curvature, $1/R - 1/R_1$ rather than the simple curvature $1/R$. The form of Eq. (3) must then be redefined as

$$k = (1/R - 1/R_1)^{1/3} \tag{16}$$

The relationship of this expression to the geometry of a partially reloaded preformed impression is illustrated in Fig. 2(b). This diagram schematically represents a partially reloaded indentation in which the dashed circle indicates the preformed spherical impression remaining when the indentation is fully unloaded. The penetration of the indenter below this dashed line is half the total elastic deformation of the preformed impression.

The geometry of a fully loaded indentation is shown schematically in Fig. 2(c).

Partially unloading an indentation from the final load $P_{\max}$ to an intermediate value P_u is wholly elastic and equivalent to reloading the residual impression to P_u. The elastic displacement may be calculated from Eq. (1), but knowledge of the relative curvature of the surfaces is required *a priori*. Fortunately, this can be avoided since the elastic component $\delta_{\max}$ and the circle of contact radius are known at full load where

$$\delta_{\max} = a_{\max}^2(1/R - 1/R_1) = a_{\max}^2 k^3 \tag{17}$$

as shown in Fig. 2(b). Consequently, the value of k required for insertion in Eq. (1) can be determined from

$$k = (\delta_{\max}/a_{\max}^2)^{1/3} \tag{18}$$

Intermediate elastic displacements are then easily determined using Eq. (1) in the form $\delta_u = Qk$.

It should be emphasized that the principal difference between the loading and unloading parts of the cycle is that the calculation of δ during loading involves a different value of k at each step while during unloading k remains fixed at the value associated with the last loading step.

The depth of penetration below the circle of contact, h_p, may include a plastic component which is substantial compared with the radius of the indenter; it must therefore be calculated using

$$h_p = R - \sqrt{(R^2 - a^2)} \tag{19}$$

The depth of the loaded indentation below the original surface during both loading and unloading is

$$h_t = h_r + \delta \tag{20}$$

and

$$h_t = h_p + \delta/2 \tag{21}$$

as shown in Fig. 2(d).

Assuming the elastic displacement of the preformed spherical impression is evenly divided above and below the circle of contact, as for the loading of a plane, the depth of the residual depression is

$$h_r = h_p - \delta/2 \tag{22}$$

IV. DETERMINING THE RADIUS OF THE CIRCLE OF CONTACT FROM MULTIPLE PARTIALLY UNLOADED INDENTATIONS

Since stepwise unloading produces a set of depth measurements which follows a law of the kind $\delta = qP^{2/3}$, in which q is a constant involving the remaining parameters of Eq. (1), only two data points are required to determine h_r: One of these is a final depth h_t and another, h_s, may be obtained by partially unloading the indentation from h_t.

Providing that the partial unloading is not too great, reloading is completely elastic, allowing the indentation to be reloaded to its original depth. It may then be further enlarged by increasing the load by another step, and partially unloading.

Forming a ratio in the form

$$(h_t - h_r)/(h_s - h_r) = (P_t/P_s)^{2/3} \tag{23}$$

allows h_r to be calculated from

$$h_r = [h_s(P_t/P_s)^{2/3} - h_t] \Big/ [(P_t/P_s)^{2/3} - 1] \tag{24}$$

Since the total elastic component $\delta = h_t - h_r$ as shown in Fig. 1(a), half of which lies above the circle of contact as shown in Fig. 2(c), the plastic component is

$$h_p = (h_t + h_r)/2 \tag{25}$$

and the radius of the circle of contact may be calculated from

$$a = \sqrt{(2Rh_p - h_p^2)} \tag{26}$$

V. DETERMINING HARDNESS AND MODULUS FROM PARTIALLY UNLOADED INDENTATIONS

Meyer's hardness is defined as the mean pressure over the circle of contact, i.e., $HM = P_m = P/\pi a^2$. Consequently, at each load step beyond the onset of full plastic flow hardness can be determined immediately from the load and the radius of the circle of contact.

The composite modulus E^* can be determined directly from

$$E^* = 3/4\ P/a\delta \tag{27}$$

VI. EXPERIMENTAL INVESTIGATION

A. Materials

Three standard Vickers microhardness blocks with nominal values of 900 HV30, 500 HV30, and 200 HV30 were chosen to illustrate this work. They were made by Yamamoto Scientific Tool Laboratory Co. Ltd., Funabashi-city, Chiba-prefecture, Japan, and are approximately 25 mm diameter by 5 mm thick. They are made from a selected steel specially treated for maximum uniformity of structure and are mirror finished by a technique that minimizes surface strain. Nominal values of 210 GPa and 0.3 were assumed for Young's modulus and Poisson's ratio in all simulations.

B. Indentation results

Indentation was carried out on the standard hardness blocks using a UMIS 2000 ultra-micro-indentation system at The National Measurement Laboratory of CSIRO, Lindfield, Australia. All three blocks were indented with spherically tipped diamond indenters of either 5 μm or 50 μm (nominal) spherical radius using load cycle tests. The hardest block was also indented using a multiple partial unloading sequence. This was carried out immediately following the load cycle sequence using the same indenter and indenting parameters.

Indentations were made in a line at 30 μm spacing near the center of each block and the multiple partial unloading run was made parallel to the load cycle run at similar spacing.

For each indentation, penetration was measured at each of 40 load steps, and the recovered depths were measured as the load was reduced to the same values on unloading. Unloading in the multiple partial unloading sequence was 50% of the current load at each step.

For each set of indentations the mean penetration and its variance were calculated at each of the 40 load steps. The variances were then averaged over all the loads in the set and the square root taken to give the standard deviation.

The UMIS-2000 makes contact with the testpiece surface at a load that is about 0.05% of its full load range; i.e., about 0.1 mN with a range of 200 mN. While this contact load is relatively small, the penetration it produces can be significant, particularly if the total penetration is small compared with the range of the instrument. The position of the indenter under the contact load is used as a measurement datum, ignoring any initial penetration, and the zero offset arising from this strategy is obvious in load cycle diagrams with low maximum loads. The simulations illustrated here have been offset by an amount corresponding to this initial penetration.

The material, the maximum load, and the indenter spherical radius used in each set of indentations were chosen to illustrate some aspect of the modeling process.

C. High *H/E* material (0.04)

1. 50 μm indenter

Figure 3 (crosses) is the mean of 5 fully elastic indentations in the hardest block using the load cycle mode and an indenter with a nominal spherical tip radius of 50 μm. The standard deviation is 1.4 nm.

A wholly elastic simulation using the nominal spherical radius of the indenter gave substantially different results (lower solid line). Three possible reasons for this departure were identified: uncertainty of the elastic modulus of the indenter material, a possible over-correction of the elastic compliance of the measuring system, and uncertainty of the actual radius of the indenter.

2. Young's modulus of the indenter material

Values of Young's modulus for diamond are variously quoted in the literature, e.g., 390 GPa–920 GPa[16] and 1050 GPa,[17] depending on crystallographic orientation, the higher values being more popular. A value of 1000 GPa was used in the current work. However, the assumption of a perfectly rigid indenter (infinitely high modulus) was not sufficient to remove the discrepancy.

3. Instrument compliance

A method for determining the compliance of the instrument and correction of the data is a feature of the software package of the UMIS-2000 system. To improve the fit it is necessary to remove the compliance correction entirely, but then a large body of other test results are invalidated.

4. Indenter radius

A good fit to the data could be obtained by increasing the spherical radius of the indenter to 115 μm (upper solid line). A slight flattening of the spherical shape over the 4.5 μm radius contact region, arising from as little as 0.11 μm of missing material at the center, is sufficient to produce an increase in spherical radius of this amount.

An interferogram of the contact region, illustrated in Fig. 4, showed the fourfold lobing typical of solids of revolution in diamond. Talystep tracings using a razor blade as a tracer also showed departures of circular geometry in different sections.

While all three of the above probably contribute to some extent, the indenter radius seemed to be the major contributor and was allowed to vary as necessary.

5. 5 μm indenter

Figure 5(a) (crosses) is the mean of 5 elastic/plastic indentations into this same block using the load cycle mode and an indenter with a nominal tip radius of 5 μm. The standard deviation was 6.6 nm. In this case the maximum load of 200 mN gives a substantial amount of deformation beyond the onset of full plastic flow.

A well-fitting simulation (solid line) was obtained when the spherical radius of the indenter was taken as 7.2 μm. The flow stress of 2.15 GPa at the onset of full plastic flow and strain hardening index of 0.15 are reasonable.[18]

6. Partial unloading

Figure 5(b) (crosses) is the mean of 10 elastic/plastic indentations into the same material using a multiple

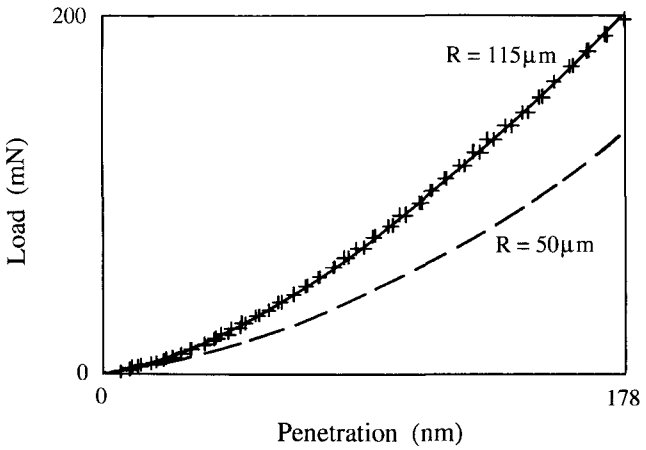

FIG. 3. Observations for the elastic loading and unloading of a steel standard hardness block (900 HV30 nominal) with a spherical indenter—50 μm nominal spherical radius—(crosses) and simulations (solid lines) with assumed radii of 50 μm and 115 μm.

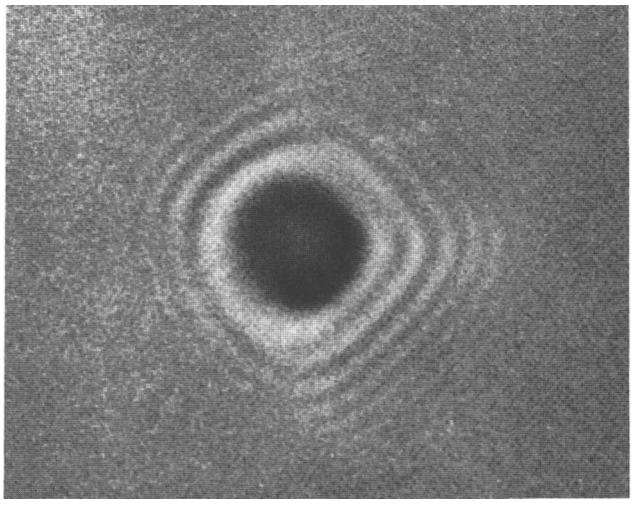

FIG. 4. Interferogram of the tip of a spherical diamond indenter–50 μm nominal spherical radius—showing the fringe pattern typical of fourfold lobing.

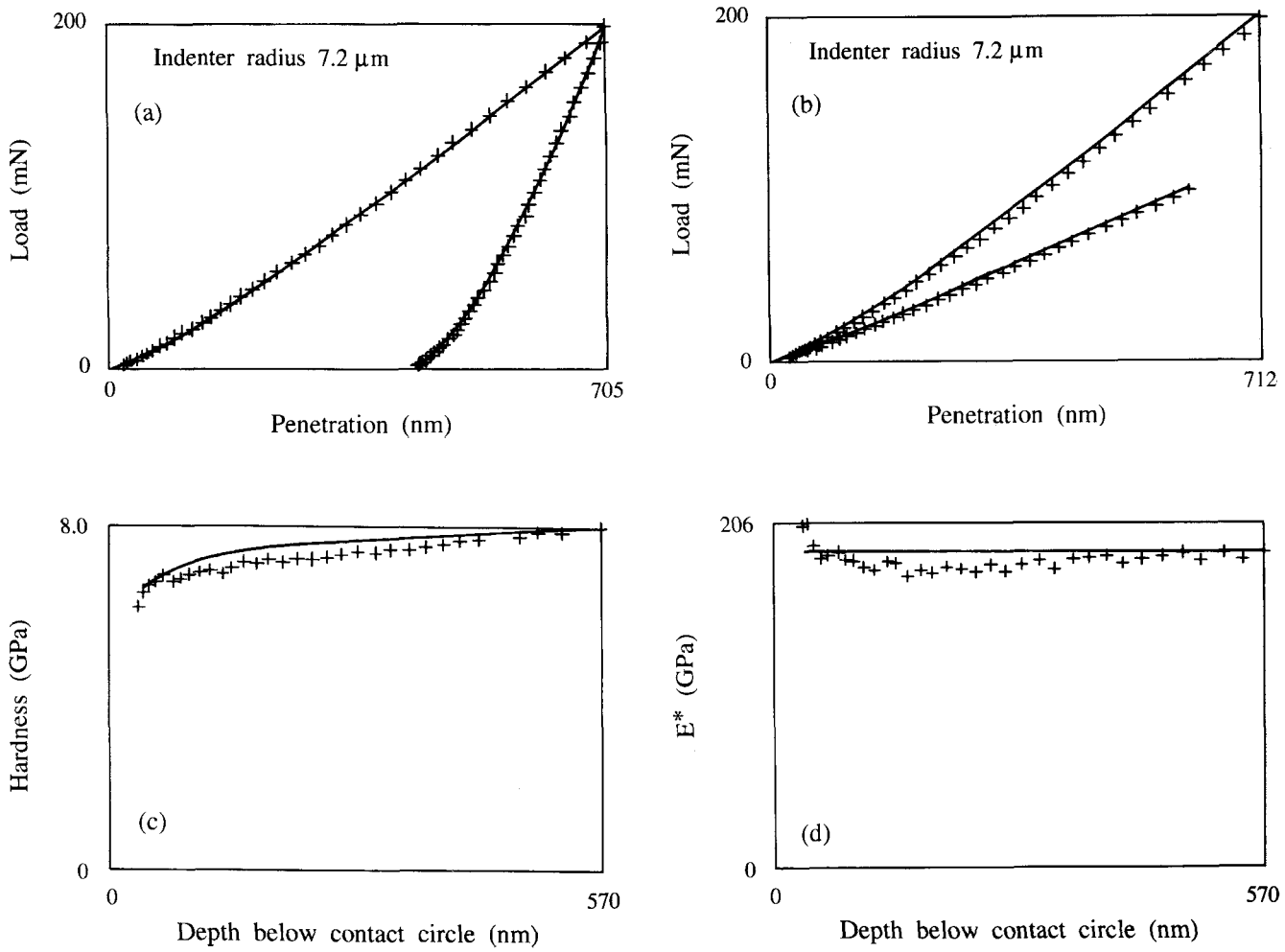

FIG. 5. (a) Observations for the elastic/plastic loading and unloading of a material with $H/E = 0.04$ with a spherical indenter—5 μm nominal radius—(crosses) and simulation (solid line). (b) Observations for a multiple partial unloading sequence for the material and conditions of Fig. 4(a) with 50% unloading (crosses) and simulation (solid line). (c) Meyer hardness as a function of penetration beyond the onset of full plastic flow determined from the observations of Fig. 4(b) (crosses) and from simulated data (solid line). (d) Composite modulus E^* as a function of penetration beyond the onset of full plastic flow determined from the observations of Fig. 4(b) (crosses) and from simulated data (solid line).

partial unloading sequence with otherwise the same indenting conditions. The standard deviation is 1.5 nm.

The simulation (solid lines) uses the material parameters and indenter spherical radius which were found to model closely the load cycle results.

7. Meyer hardness

Figure 5(c) (crosses) is a plot of Meyer's hardness versus depth of penetration below the circle of contact determined from the measured multiple partial unloading data. The solid line is the expected hardness distribution for a material with the parameters that closely model the load cycle data. The slightly lower hardness produced by the multiple partial unloading data is due to the slightly greater penetrations obtained.

8. E^* modulus

Figure 5(d) (crosses) is a plot of the composite modulus E^* versus the depth of penetration below the circle of contact calculated from the measured partial unloading data. The solid line is the composite modulus expected for the material. The result is again slightly affected by the greater penetration associated with the multiple partial unloading data.

In calculating hardness and modulus the offset of the depth measurement zero must be corrected; i.e., the amount of penetration produced by the initial contact load must be added to all measured values. The first few increments of penetration are almost always elastic for spherical indenters and the penetration can be estimated from the intercept of a linear regression of the first few

penetration measurements, on force raised to the 2/3 power.

D. Medium *H/E* material (0.02)

5 μm indenter

Figure 6 (crosses) is the mean of 5 elastic/plastic indentations into the nominally 500 HV30 block using a different indenter with a nominal spherical tip radius of 5 μm (the previous indenter of this radius having been damaged). The standard deviation is 2.6 nm.

The simulation (solid line) is a good fit when the effective spherical radius of the indenter is taken as 5.95 μm. The 1.25 GPa flow stress at the onset of full plastic flow and strain hardening index of 0.17 are again reasonable.

E. Low material *H/E* (0.009)

Figure 7 (crosses) is the mean of 7 elastic/plastic indentations into a low H/E material (the 200 HV30 block) using the load cycle mode and the nominally 50 μm radius indenter. The standard deviation is 1.6 nm. The maximum load was again chosen to give a substantial deformation beyond the onset of full plastic flow.

A reasonably well-fitting simulation (solid line) was obtained with an indenter radius of 97 μm, the somewhat smaller value than that found in Fig. 3 being attributed to the smaller circle of contact. The 0.18 GPa flow stress at the onset of full plastic flow and higher strain hardening index of 0.35 are again reasonable.

VII. DISCUSSION

The following should be considered when selecting indenting conditions and choosing parameters for simulation.

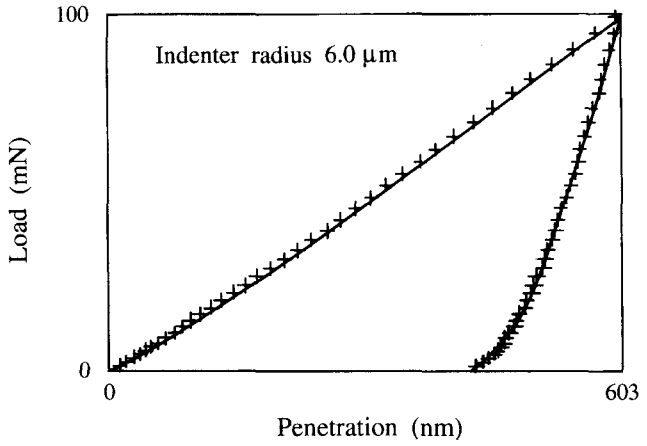

FIG. 6. Observations for the elastic/plastic loading and unloading of a material with $H/E = 0.02$ with a spherical indenter—5 μm nominal radius—(crosses) and simulation (solid line).

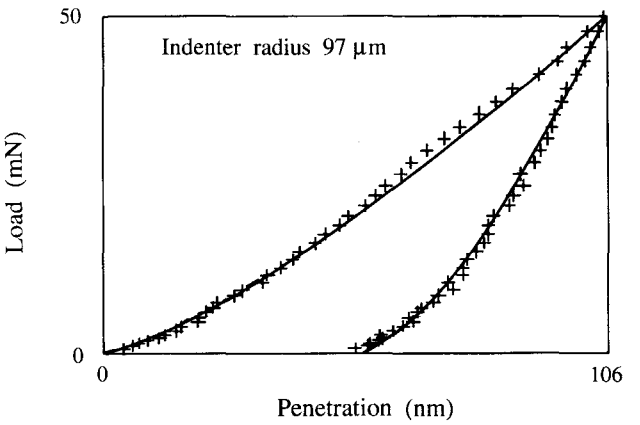

FIG. 7. Observations for the elastic/plastic loading and unloading of a material with $H/E = 0.009$ with a spherical indenter—50 μm nominal radius—(crosses) and simulation (solid line).

A. Indenter radius

The spherical radius of the indenter, in conjunction with the flow stress at the onset of full plastic flow, determines the load at which the behavior changes from wholly elastic to elastic/plastic. A suitable indenter spherical radius for an actual indentation sequence may be chosen by simulating its behavior beforehand. However, for better agreement better methods of manufacturing and measuring small spherical radii are still required.

B. Estimation of material properties

Material properties may or may not be known *a priori*. If they are, simulation can proceed immediately; otherwise they must be estimated in some way. A good fit to indentation results may require iteration of all four material parameters and possibly indenter radius. An assessment of Young's modulus can, however, be made from the unloading data using the method described for partial unloaded data.

C. Estimating flow stress at the onset of full plastic flow

Tabor[10] showed that for a Vickers indentation $P_m/Y_r = 2.8$ when Y_r is the representative yield stress determined at a representative strain of 0.08. If the material strain hardens according to a power law from first yield, the representative flow stress for a spherical indentation at the onset of full plastic flow is given by

$$Y_c = Y_{0.08}(2.5\ a_c/R)^x \tag{28}$$

Using Eqs. (1) and $P_c = 3\pi a_c^2 Y_c$

$$a_c/R = 9\pi Y_c/4E^* \tag{29}$$

On substituting in Eq. (27)

$$Y_c = (45\pi/8)^{x/(1-x)} Y_{0.08}^{1/(1-x)} \quad (30)$$

In some materials, in particular some steels, the onset of yielding is obscured by an anomalous region. For these materials it is generally not possible to determine a representative flow stress at the onset of full plastic flow in this way. In these cases a well-established value for Y_c and x can be determined from a stress strain curve.

The plot of hardness versus penetration obtained from multiple partial unloading is in some sense similar to the stress strain curve. Hardness and mean pressure are equivalent, and related to representative yield stress. Penetration, beyond the onset of plastic flow, is related to Tabor's[10] parameter a/R, which he uses as a measure of representative strain. Therefore, hardness at the onset of plastic flow indicates the value of the initial yield stress while an increasing hardness with penetration indicates strain hardening behavior.

D. The effect of displaced material

Material displaced by indentation is sometimes found piled up around the indentation. According to Mott[19] this piled-up material supports little or no load. A recent study by LaFontaine *et al.*[20] involving Vickers indentation supported this view. If this is generally true, the disposition of displaced material should not affect the conclusions reached in this work. However, a general uplifting of material beneath and around the indentation would tend to reduce measured depths and lead to overestimation of depth by the simulation technique. It is also possible for general uplifting to inflate the estimation of strain hardening since both tend to reduce measured depths as penetration increases. It may also mask the indentation size effect commonly observed in hardness testing with low loads which normally increases hardness values as indentation size is decreased.

E. Simulation in the elastic/plastic transition stage ($1.1 < P_m/Y < 3.0$)

There is as yet no simple way of describing the mechanism by which strain is accumulated during the transition from fully elastic to fully plastic indentation. Consequently, there is no way of calculating the depth of the residual depression remaining after unloading from a load in this range. The model assumes full elastic recovery up to $P_m/Y = 3.0$ and is, therefore, unsatisfactory for investigating indentations that terminate within this region. Further work is being undertaken to investigate this aspect of indentation.

VIII. CONCLUSIONS

A simple analytical model has been proposed that simulates the entire loading and unloading sequences of continuous load cycle indentation, or the alternating loading and unloading sequences of indentation with multiple partial unloading, using a spherical indenter. The model is easily programmed on an ordinary PC and may be used to simulate or analyze data generated with an ultra-micro-indentation system, a micro-indentation system, or the macro-indentation force versus displacement data obtained with a universal testing machine. Simulated results agree very well when compared with actual data obtained with a stepwise loading and unloading instrument such as the UMIS-2000. By varying such parameters as Young's modulus, Poisson's ratio, flow stress at the onset of full plastic flow, and the strain index, indentation behavior can be explored. This then allows the—often subtle—differences in the measured data to be understood better.

A technique has also been proposed by which hardness and a composite form of the elastic modulus may be obtained from the final load of load cycle indentation sequences or as a function of depth of penetration from multiple partial unloading sequences. These techniques are valuable in determining the mechanical properties of near surface materials and coatings.

ACKNOWLEDGMENTS

The authors wish to acknowledge the contribution of Mr. F. Lesha, whose measurements of indenter shapes were invaluable.

REFERENCES

1. T. J. Bell, A. Bendeli, J. S. Field, M. V. Swain, and E. G. Thwaite, Metrologia **28**, 463 (1991/92).
2. R. Hill, E. H. Lee, and S. J. Tupper, Proc. R. Soc. **A188,** 273 (1947).
3. L. E. Samuels, in *Microindentation in Metals, Microindentation Techniques in Materials Science and Engineering,* edited by P. J. Blau and B. R. Lawn (ASTM Special Technical Publication, 1985), p. 889.
4. M. C. Shaw and G. J. DeSalvo, Trans. Am. Soc. Mech. Eng., Series **B92**, 480 (1970).
5. T. O. Mulhearn, J. Mech. and Phys. of Solids **7**, 85 (1959).
6. H. A. Francis, Trans. of the ASME, July 272 (1976).
7. P. S. Follansbee and G. B. Sinclair, Int. J. Solids and Structures **20**, 172 (1981).
8. K. L. Johnson, *Contact Mechanics* (Cambridge University Press, 1985).
9. I. N. Sneddon, Int. J. Eng. Sci. **3**, 47 (1965).
10. D. Tabor, *Hardness of Solids* (Oxford University Press, 1951).
11. L. E. Goodman and L. M. Keer, Int. J. Solids and Structures I **407**, 117 (1965).
12. A. E. H. Love, *A Treatise on the Mathematical Theory of Elasticity,* 4th ed. (Cambridge University Press).
13. M. J. Puttock and E. G. Thwaite, *Elastic Compression of Spheres and Cylinders at Point and Line Contact,* National Standards

Laboratory Technical Paper No. 25 (Commonwealth Scientific and Industrial Research Organization, Australia, 1969).
14. A. I. Nadai, *Theory of Flow and Fracture of Solids* (McGraw-Hill, New York, 1963), Vol. 2, p. 221.
15. E. Meyer, Z. Ver Deutch Ing. **52**, 645 (1908).
16. M. V. Sinnott, *The Solid State for Engineers* (John Wiley and Sons Inc., New York, 1961).
17. *The Properties of Diamond,* edited by J. E. Field (Academic Press, London, 1979).
18. A. G. Guy and J. J. Hren, *Elements of Physical Metallurgy,* 3rd ed. (Addison-Wesley Pub. Co., Reading, MA, 1974), p. 138.
19. B. W. Mott, *Microhardness–Indentation Hardness Testing* (Butterworths, London, 1956).
20. W. R. LaFontaine, B. Yost, and Che-Yu Li, J. Mater. Res. **5**, 776 (1990).